crystals

MDPI

Article

A Novel Combining Method for Composite Groove Structure Fabrication

Shuhai Huang [1,†], Cheng Chang [2,†], Jiaqi Liu [3], Shouwei Tong [1], Shouzheng Sun [2], Zhenyu Han [2], Qiang Chen [1,*] and Xudong Ran [1,*]

[1] Southwest Technology and Engineering Research Institute, Chongqing 400039, China; hsh82@163.com (S.H.); zsl199605@163.com (S.T.)
[2] School of Mechatronics Engineering, Harbin Institute of Technology, Harbin 150001, China; 21b908116@stu.hit.edu.cn (C.C.); szsun@hit.edu.cn (S.S.); hanzy@hit.edu.cn (Z.H.)
[3] Chang Guang Satellite Technology Co., Ltd., Changchun 130000, China; liujiaqi1004@jl1.cn
* Correspondence: 2009chenqiang@163.com (Q.C.); xudongran0828@outlook.com (X.R.); Tel.: +86-023-68792167 (X.R.)
† These authors contributed equally to this work.

Abstract: A composite groove structure with high specific strength and light weight has great potential in industrial application, but few studies on this have been carried out due to the fact that it is difficult to fabricate by one of the existing methods. The purpose of this work was to propose a novel method combining 3D printing and filament winding to manufacture the groove structure and study the link between its mechanical strength needs and fabrication parameters. Specifically, filament winding and 3D printing were used to fabricate the cylinder part and complex ring slot part of the groove structure, which is difficult to fabricate by winding. The combining method took advantage of the winding's high efficiency and the printing's high forming degree of freedom. The specimen was taken from the structure and submitted to a short beam test to determine its interlaminar shear strength, whereas thermal tests were carried out to evaluate its mechanical performance under high temperature. The interlaminar shear strength reached 6.694 MPa at a fiber orientation of 90°, a heating temperature of 245 °C and a thickness of 0.5 mm. The SEM photo showed some voids and gaps and typical failure in the failed specimen. DMA and TGA were carried out to investigate the performance under high temperature, from which the storage modulus lost half to 120 °C. Overall, the proposed combining novel method offers a new direction in the fabrication of continuous fiber-reinforced thermoplastic composites' groove structure.

Keywords: filament winding; 3D printing; combining method; interlaminar shear strength

check for updates

Citation: Huang, S.; Chang, C.; Liu, J.; Tong, S.; Sun, S.; Han, Z.; Chen, Q.; Ran, X. A Novel Combining Method for Composite Groove Structure Fabrication. *Crystals* **2023**, *13*, 1644. https://doi.org/10.3390/cryst13121644

Academic Editor: Pavel Lukáč

Received: 7 October 2023
Revised: 23 November 2023
Accepted: 25 November 2023
Published: 28 November 2023

Copyright: © 2023 by the authors. Licensee MDPI, Basel, Switzerland. This article is an open access article distributed under the terms and conditions of the Creative Commons Attribution (CC BY) license (https://creativecommons.org/licenses/by/4.0/).

1. Introduction

Groove structure is an important structural part in aircrafts, which not only occupies a large proportion in the aerospace field, but also has a high frequency of use in other fields such as the internal combustion engine piston oil groove, pass roll, rope groove roller, etc., in which the structure is vulnerable [1]. The groove structure is normally made of a high-strength alloy. With the application of continuous fiber-reinforced composites in aerospace, automobile manufacturing, construction and other fields [2], composites are used to fabricate a light-weight and high-strength groove structure. Generally, the reinforcement fiber part can be divided into a short fiber and a long continuous fiber. To reach a high performance level, the long continuous fiber's reinforcement is needed. However, it increases the complexity of the processing. Additionally, it is also hard to finish the fabrication ensuring efficiency and mechanical strength on special direction by only one composite fabrication method. Currently, many composite additive manufacturing methods have been developed, such as filament winding, placement, thermal compressing, pultrusion and 3D printing, among which filament winding is a traditional continuous fiber

processing method with the highest efficiency. Moreover, continuous fiber 3D printing is now advanced, with its advantage of high trajectory design freedom for complicated parts. Consequently, for groove structures with typical winding features and complex parts, a combining method of filament winding and 3D printing with continuous fiber is proposed to solve the complexity of the fabrication and ensure the processing efficiency.

Filament winding is the main molding process for manufacturing rotary composite components [3]. It has the advantages of high forming efficiency, high forming quality and good mechanical properties when making the structure with rotary characteristics, and has shown great potential in improving the performance of composite materials and reducing production costs [4–7], so it is widely used in various fields of composite manufacturing. For example, in the aerospace field, SRM combustion chamber shells, liquid propellant storage tanks, solid missile launch canisters and various high-performance pressure vessels are obtained by the winding process [6]. The composite pressure vessel is a typical filament-wound component. Aleksander et al. studied the manufacturing process focusing on the parameter of fiber tension. The result showed that the increase in fiber tension led to higher burst pressure and mechanical properties [8]. Eduardo et al. also took the winding pattern information as an intrinsic characteristic of the components manufactured by filament winding and studied its influence on the mechanical behavior of the wound cylinders. It was found that the influence was different under different loading cases [9]. Instead of investigating the traditional winding parameters, Rahmad et al. analyzed the stress of the mandrel shaft used in filament winding to determine the deflection of the mandrel, which influences the quality of the wound components. The highest value of von Mises stress was 217.41 MPa under the load of 200 N [10]. Other than studies on how to improve the quality of the wound components, the University of Stuttgart developed a new rotating-part winding method—the assembly core method [11], which is an extension of filament winding. This method can achieve complex structures by dividing the whole surface into discrete segments, and then combining these discrete segments into a whole convex shape to assemble the core geometry. A synchronous elastic surface is regenerated to connect these discrete segments. The geometry of the assembled core is derived from the entwined fiber corners. The fabricated laminates completely cover the core after winding, so these discrete segments must be separated from the laminate by milling. The final geometry is assembled from the fabricated discrete segments. Because the process relies on segmentation, it is not suitable for machining shell structures with complex geometries on a single winding mandrel.

Three-dimensional printing technology is a layer-by-layer printing process using adhesive materials that can make use of various materials to fabricate a variety of complex geometric structures [12–14]; it is an intelligent manufacturing technology that can realize the rapid manufacturing process using three-dimensional parts. The biggest feature of 3D printing technology is its designability, which means it can print out parts with various morphologies and complex structures [15,16]. Three-dimensional printing technology greatly improves the freedom of part design, provides a new method for manufacturing complex parts, makes the manufacturing of complex parts simpler and faster, and broadens the creativity of mechanical structure design. Additionally, 3D printing using carbon fiber and resin material which also improves the fabricated parts' strength which solves the common problem of low mechanical performance of traditional 3D resin printing. Hou et al. tailored the local properties of continuous fiber-reinforced heterogeneous composites through fiber arrangement design to maximize the load and fiber utilization efficiency. The flexural strength of the printed components reached 207 MPa and the maximum increase was 115% compared with that before optimization [17]. The 3D printer prepared by Li et al. [18] can print continuous fiber-reinforced materials. The 3D printer designed by the team is mainly used to print continuous carbon fiber-reinforced polylactic acid composites with a curved structure with higher mechanical strength. The experimental results show that the nozzle design can be used for the printing and processing of uniformly mixed carbon fiber and Polylactic Acid (PLA), which can achieve straight and curved paths for continuous

carbon fiber-reinforced composite 3D printing. Based on the traditional continuous fiber 3D print head, Pruss et al. [19] designed a 3D print head with three ports (top and side), and provided a heated mixing chamber at the center of the print head. Two channels were embedded on both sides of the original head to enable continuous fiber-reinforced material printing. This three-port print head can both take advantage of the design freedom of AM and of controlling the material properties of the deposited composite. In addition, Pruss also proposed several printing modes, including the cellular printing mode to reduce the support material, the load-based printing mode and the selective support mode. Zhang Peng et al. [20] explored the mechanical properties of carbon fiber-reinforced polypropylene plastic (PP) printed parts by using a three-extrusion 3D printer with online impregnation; they established a model of the material line width during printing and conducted predictive analysis and verified it through experiments. In addition, they also studied the printing temperature, printing speed, fiber content and interlayer thickness's effects on the bending strength and bending modulus of specimens. Although the carbon fiber reinforcement improves the fabricated parts' mechanical performance, continuous carbon fiber 3D printing's speed is limited at 2 mm/s~5 mm/s, which restricts its wide use. The discussed studies have been summarized in Table 1.

Table 1. Winding and printing research.

Method	Focus	Reference
Filament winding	Fiber tension's influence on mechanical performance of pressure vessel	[8]
	Winding pattern's influence on mechanical performance	[9]
	Mandrel shaft's stress influence	[10]
	Assembly core method for complex surface	[11]
Continuous Fiber 3D printing	Parameter optimization based on load	[17]
	Curve structure printing	[18]
	Three-port printing head and different printing mode	[19]
	Line width prediction model	[20]

Although the filament winding and 3D printing methods have been developed a lot, winding is still limited at the rotating part fabrication and the efficiency of continuous fiber printing is limited while other composite manufacturing method also have their own limitation. Therefore, some researchers have conducted a few investigations to attempt to combine different fabrication methods to manufacture composite parts, which are generally undertaken with one method. Mohammad Rakhshbahar proposed a novel approach combining automated fiber placement(AFP) and additive layer manufacturing to improve the efficiency and lower the cost. In this method, additive layer manufacturing—that is, 3D printing—was used to fill the gaps occurring inevitably during automated fiber placement to overcome this drawback and ensure the composite parts could be manufactured in a homogeneous manner. And the strength of the fabricated part was almost equal to the perfect no-gap AFP part [21]. Rajkumar et al. combined the AFP and 3D printing from a different perspective. According to the requirements of the complex geometry composite structure for AFP, 3D printing becomes the most suitable way for rapid tool production. Then AFP can proceed on the printed substrate tool. PEI and ASA composite planes are fabricated, and the highest modulus of elasticity can reach 39.40 Gpa and 31.55 Gpa, respectively [22].

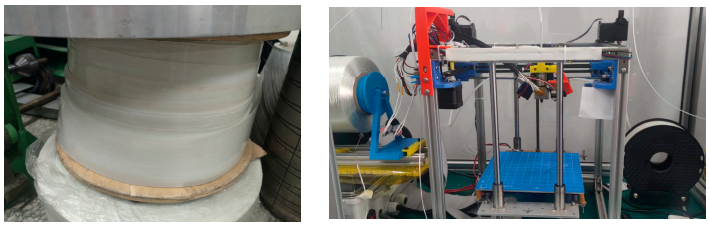
Although a few researchers have begun to study the combination of different composite manufacturing methods, the research is still limited and small in number. For the manufacturing of the groove structure in this paper, due to its special geometric structure, it needs hoop strength and axial strength vertical to the slot. As discussed in the aforementioned review, filament winding is suitable to fabricate rotating parts where hoop strength is needed, while 3D printing can manufacture complex structures rapidly. Therefore, a

novel method combining filament winding and 3D printing is proposed to apply to the groove structure manufacture process. It could not only improve the processing efficiency of the component but also ensure its mechanical properties. This new type of processing method would make it possible to process the groove type structure quickly and with high quality, and provide a new idea for complex composite structure fabrication.

2. Materials and Methods

2.1. Material Preparation

Continuous glass fiber and polypropylene (PP) were chosen as the reinforcement fibers and resin matrix for its ease of processing, low associated costs and high volume processing potential and performance [23]. The glass fiber prepreg for winding is produced by Nanjing Special Plastic Composite Material Co. LTD with a resin content of 55%, surface density of 200 g/m^2, tensile strength of 1074 Mpa and tensile modulus of 107 Gpa. The belt was cut in the typical used prepreg size of 6.35 mm width. Figure 1a shows the prepreg used. The resin matrix polypropylene was a thermoplastic material, and the melting point of the prepreg was about 174 °C as tested by the DSC test. The printing material was manufactured by the material extrusion type online impregnation 3D printing equipment, as shown in Figure 1b. The polypropylene filament (Hailuohao, Zhejiang, China) with a diameter of 1.75 mm was used as the resin matrix for the printing wire while the glass fiber used was 240 TEX bought from Nanjing Fiberglass Research & Design Institute Co. Ltd. In Nanjing China. The diameter of the extruded prepreg wire was about 1.2 mm~1.5 mm, which is usually used in the continuous fiber printing.

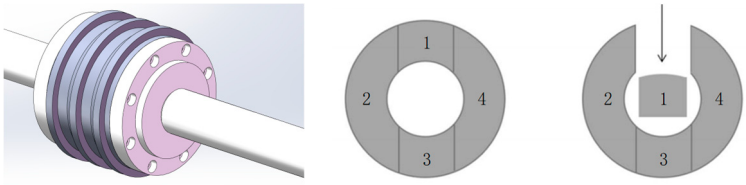


(**a**) (**b**)

Figure 1. Material: (**a**) glass fiber-reinforced polypropylene (PP) prepreg; (**b**) online impregnation 3D printing equipment.

2.2. Mold Design

The mold used in the experiment was made of 6061 aluminum alloy with good thermal conductivity, corrosion resistance and medium strength, where heat-resistant paper tape and adhesive were placed. The heating source of the mold was an attached silicone heating sheet. The split mold was designed in four parts to make it easy for mold release, as shown in Figure 2. The fabrication process was to print the groove shape structure until it formed a completed cylinder outside the shape first and turn the end effector to the filament winding device to finish the ring winding process. Then parts one and three of the mold could be removed and the other two parts could be taken down to ensure the integrity of the groove structure. The filament and prepreg wire trajectory of the winding and printing process are shown in Figure 3.



(**a**) (**b**)

Figure 2. Schematic of removable mold: (**a**) 3d model; (**b**) split mold design.

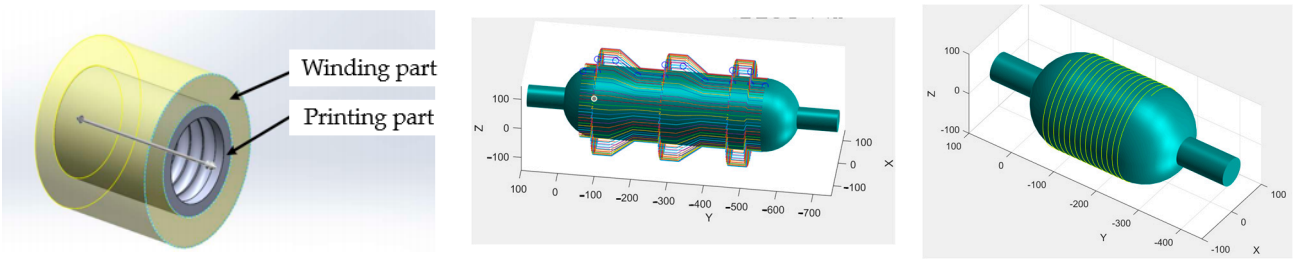


Figure 3. Schematic of winding and printing trajectory: (**a**) the groove structure; (**b**) winding trajectory; (**c**) printing trajectory.

2.3. Designed Equipment and Processing

In order to realize the combining method, special equipment was designed. The equipment was a robot with an end effector combining filament winding and the 3D printing device to finish the whole process, as shown in Figure 4. The robot was KUKA KR210-R2700; the end effector was self-designed with two functional parts, which improved the integrity and flexibility of the method. The filament part included air heating, tension control, a feeding and filament guiding device and a printing part which consisted of heating, extruding and a cutting device, as shown in Figure 5.

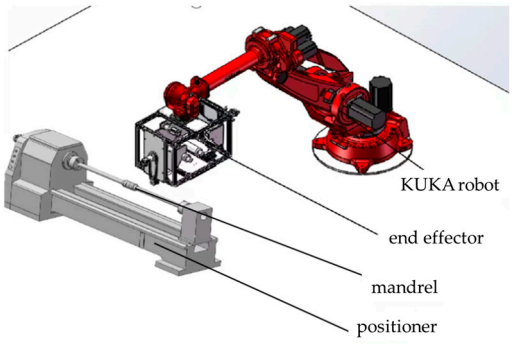


Figure 4. Schematic of the equipment.

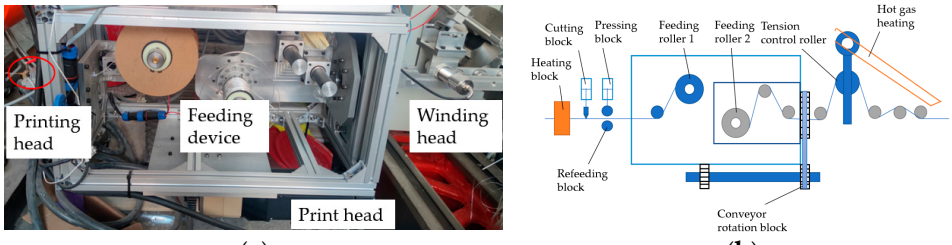


Figure 5. End effector: (**a**) picture of the end effector; (**b**) schematic of the end effector.

2.3.1. Filament Winding Device

As opposed to traditional fiber winding, some special parts needed to be justified to adapt to the glass fiber-reinforced PP resin prepreg belt winding. During the winding process, the magnitude of the tension affects the quality of the finished product, so in the winding process, the tension was controlled to be kept it at an appropriate and constant value. The tension control system designed according to the control requirements is shown in Figure 6a, wherein the PP prepreg belt was wound on the tray, the tray was tightened and fixed through the air expansion shaft, the air expansion shaft was connected to the tension motor through the flange, the tension motor released yarns on the tray through rotation and the prepreg belt was wound around the tension sensor through the guiding

roller. Finally, the belt was put through three slotted rollers, which were used to maintain the belt shape, and was wrapped around the mandrel. The winding nozzle was designed to ensure that the tow fed through could be wound with a certain tension and a certain direction, as shown in Figure 6b,c. And, the heating of the filament was performed with a hot gas gun.

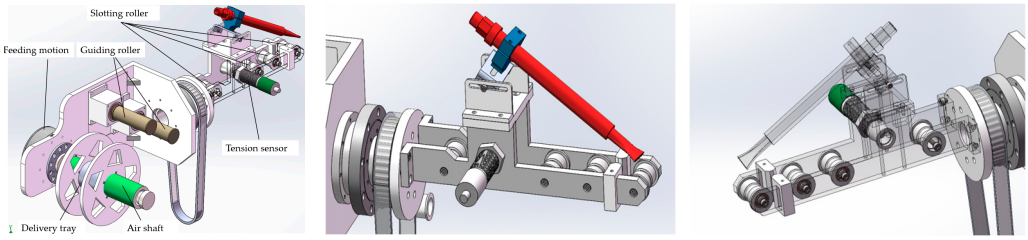


Figure 6. Schematic of the winding head: (**a**) tension control system; (**b**) winding nozzle; (**c**) guiding roller with slot.

2.3.2. 3D Printing Device

In order to achieve the continuous fiber 3D printing, a printing device with a cutting tool, heating block and feeding part was applied, as shown in Figure 7. As opposed to the current continuous fiber printing device, the prepreg wire needed to be cut at a specific position to maintain the continuous processing in 3D printing and the need to switch printing trajectory. The cutting tool was driven by an air shaft to cut the wire at the gap in the middle of the throat pipe, as shown in Figure 7a,b. The refeed system consisted of two refeed rollers, one was an active roller driven by a servo motor, and the other was a driven roller driven by a single cylinder, which provided the feeding force and clamp function, respectively, as shown in Figure 7c. The heating block was located at the start of the nozzle, which contained the heat dissipation and insulation blocks to prevent heat affecting the feeding and transfer to the servo motor on the backboard, as shown in Figure 7d.

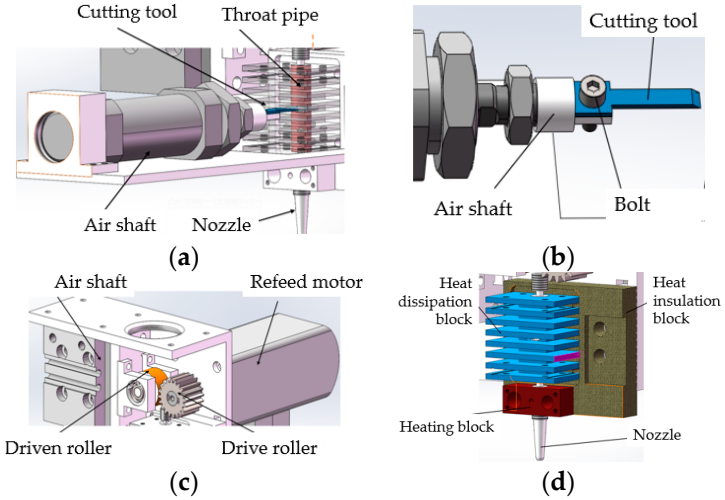


Figure 7. Schematic of the printing head: (**a**) cutting mechanism; (**b**) cutting tool; (**c**) refeeding mechanism; (**d**) heating system.

3. Test Results

3.1. Specimen Preparation

In this paper, the JC/T 773-2010 Building Materials Industry Standard of the People's Republic of China: Fiber Reinforced Plastics—Short Beam Method was used to determine

the interlayer shear strength [24]. According to the JC/T 773-2010's fiber-reinforced plastics interlayer shear strength test method, the shape of the specimen is shown in Figure 8.

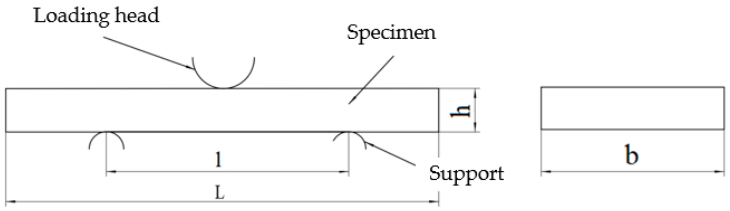


Figure 8. Schematic of the test standard.

In this standard, specimen thickness h = (2 ± 0.2) mm, width b = (10 ± 0.5) mm, specimen length L = (20 ± 1) mm. In this experiment, the thickness h was 2 mm, the measurement span was 10 mm, the length of the specimens was 20 mm, the width was 10 mm, the number of specimens in each group was eight and the speed of the applied force was 1 mm/min. The circle part of the groove structure for bearing was selected to be cut to eight specimens. The specimen location is shown in Figure 9. The blue part is the location of the cut specimen.

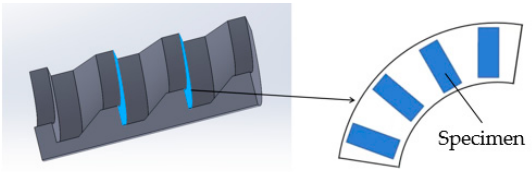


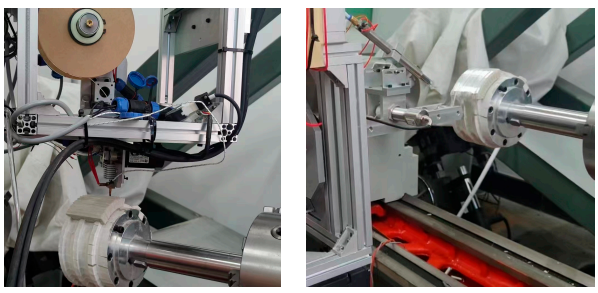
Figure 9. Schematic of the specimen location.

3.2. Testing Methods

3.2.1. Experiment Design

In this paper, the three factors of temperature, layer thickness and fiber direction were primarily explored in the production of the specimens. The orthogonal experimental method was adopted for exploration. The orthogonal experiment with multi-factor tests was designed according to orthogenicity [25]. The orthogonal factors of this experiment were determined through investigation and analysis, and three factors, namely fiber direction, printing temperature and printing layer thickness, were selected for the experiment at two levels, as shown in Table 1. Fiber direction is related to the structure's mechanical performance along specific directions while temperature and thickness influence the interlaminar bonding. The selected levels were based on the primary experiment.

The L4 (3 × 2) orthogonal experiment table was adopted, and the orthogonal experiment table was designed according to the selected experimental factors and levels as shown in Table 2. The processing was as shown in Figure 10.



(**a**) (**b**)

Figure 10. Processing: (**a**) printing; (**b**) winding.

Table 2. Experimental factors and levels.

Level	Fiber Direction	Temperature	Thickness
1	0°	225 °C	0.5 mm
2	90°	245 °C	1 mm

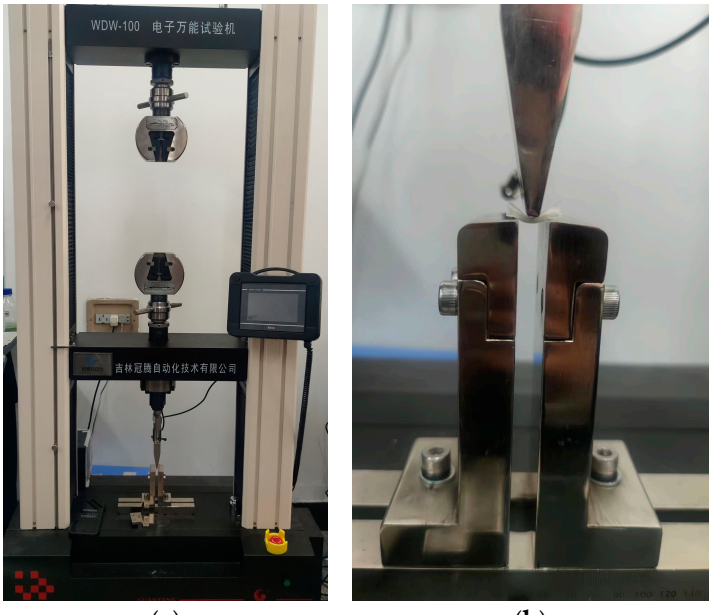
3.2.2. Interlaminar Shear Test

According to the parameters in the orthogonal experiment table, eight samples were cut out, and each sample was cut into a rectangular square with a width of 10 mm, thickness of 2 mm and length of 20 mm. The four groups of cut samples are shown in Figure 11. The eight samples in each group were numbered. For example, the eight samples in No.1 were 1–1, 1–2, 1–3, 1–4, 1–5, 1–6, 1–7, 1–8.



Figure 11. Cut specimens of four groups.

The testing instrument used in this experiment was a universal testing machine, as shown in Figure 12a. The main bearing force of the structure is the transverse shear force. Therefore, the interlayer shear performance of the samples was tested in this experiment. The distance between the two test supports of the testing machine was adjusted to 10 mm, and the cut rectangular specimen was placed on the two supports as a simple supported beam. The lowering speed of the testing machine was 1 mm/min, and the load was applied to the center of the test piece, as shown in Figure 12b. The force curve of the test piece during interlayer shear was recorded for data processing. The failed specimens are shown in Figure 13.



(**a**) (**b**)

Figure 12. ILSS Test: (**a**) universal testing machine; (**b**) test process.



(**a**) (**b**)

Figure 13. Interlayer shear failure diagram of sample: (**a**) failure diagram of 0° specimen; (**b**) failure diagram of 90° specimen.

3.2.3. Test Result

There were four samples in each test group. Each test group was tested eight times, and the test curve of the interlayer shear strength of the eight test groups was obtained through the test, as shown in Figure 14.

By calculating the average value of the eight samples in the horizontal groups of each factor, the interlaminar shear strength of each group was obtained, and a bar chart was drawn, as shown in Figure 15, from which the mean value and error fluctuation of the four groups of interlaminar shear strength could be directly seen.

The orthogonal experiment table is shown in Table 3. Through the analysis of the results in the table, it was found that the fiber direction of 90°, the printing temperature of 245 °C, and the layer thickness of 0.5 mm was the optimal parameter combination in the test. At the same time, through calculation and comparison, it can be concluded that among the three influencing factors, the fiber direction was the most important influencing factor, followed by the printing layer thickness and the printing temperature.

Table 3. ILSS test results.

No \ Factor	Fiber Direction	Temperature	Thickness	ILSS (MPa)
1	0°	225 °C	0.5	1.031
2	0°	245 °C	1	0.663
3	90°	225 °C	1	5.414
4	90°	245 °C	0.5	6.694
K_{1q}	0.847	3.223	3.863	
K_{2q}	6.054	3.679	3.039	
Rq	5.207	0.456	0.842	

The experimental data were filled into the orthogonal experiment table as shown in Table 3. K_{1q} and K_{2q} in Table 3 represented the average influence of the corresponding experimental factors at each level. For example, the average interlaminar shear strength of the two groups of tests at 90° of the fiber orientation factor was 6.054 MPa, and through the analysis and calculation of the test results in the table and from the K1q and K2q values, it was found that the fiber direction of 90°, the printing temperature of 245 °C and the layer thickness of 0.5 mm was the optimal parameter combination under the test conditions. In the test table, Rq was the range of the mean response of each factor, and the larger the Rq was, the more obvious the influence of this factor on the test results. Through the calculation and comparison of Rq, it was observed that among the three influencing factors, the fiber direction was the most important one; the thickness of the printing layer was the second.

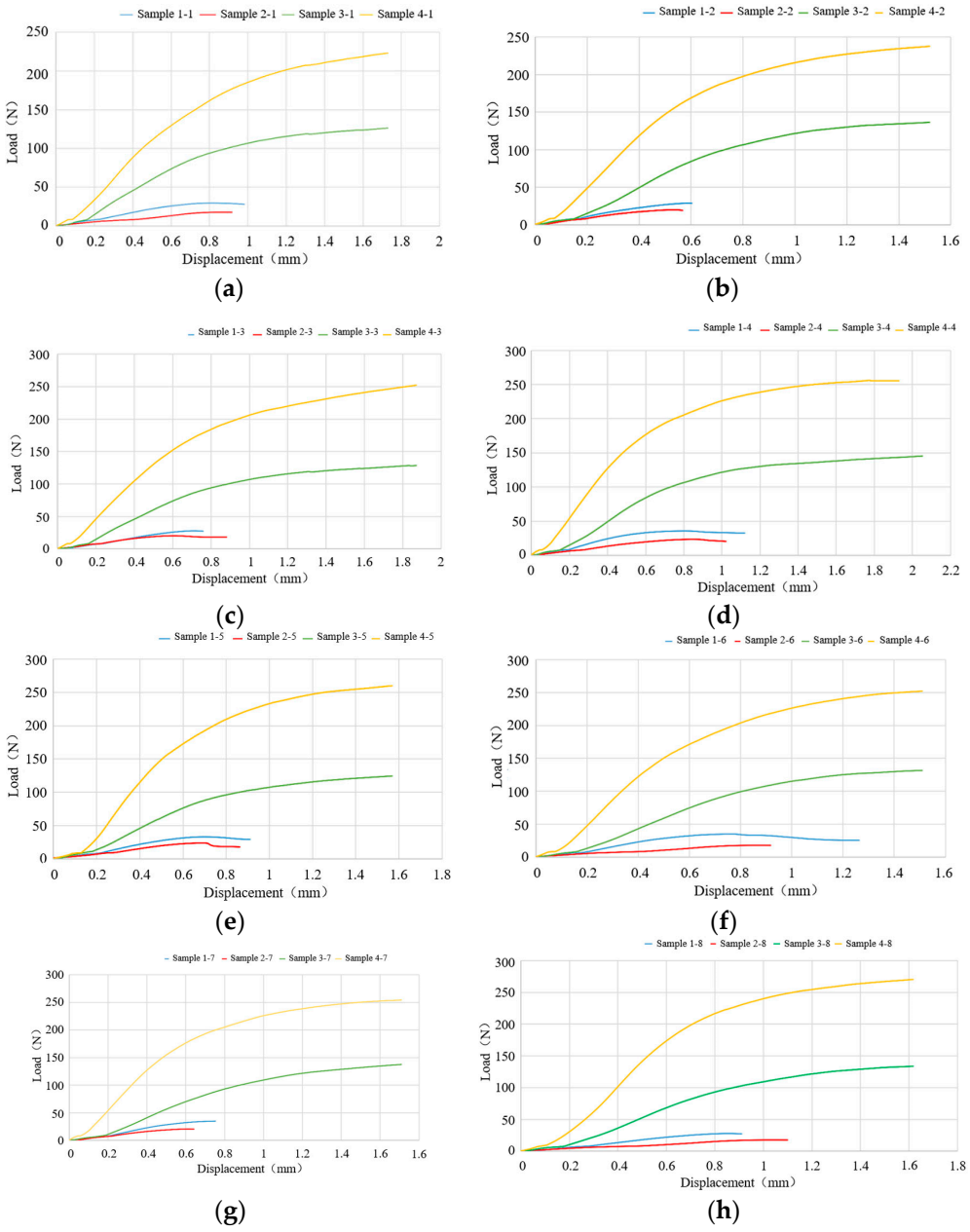


Figure 14. The test's load–displacement curves: (**a**) curve of No. 1 group; (**b**) curve of No. 2 group; (**c**) curve of No. 3 group; (**d**) curve of No. 4 group; (**e**) curve of No. 5 group; (**f**) curve of No. 6 group; (**g**) curve of No. 7 group; (**h**) curve of No. 8 group.

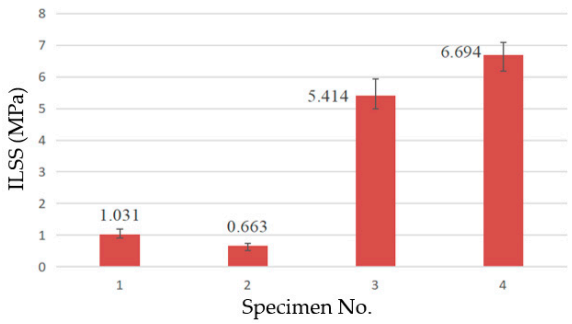


Figure 15. ILSS histogram.

3.2.4. Microscope Inspection

The micromorphology of the specimen determines the macroscopic mechanical properties. The microscopic photo was observed, and then analyzed. Zeiss Gemini-560 field emission scanning electron microscopy, as shown in Figure 16, was used for microscopic observation. The SEM photos are shown in Figure 17. Figure 17a illustrates the bonding mechanism of the cross-sectional micro-structure of the part printed with 90° fiber orientation. It can be observed that some voids existed in the specimen while the other parts showed good interfacial bonding between the glass fiber and PP resin. In Figure 17b, the void and gap can be observed clearly. Figure 17c,d show the micro-structure of the specimen's cross section and side view after the shear test. The separation between the layers is obvious which means the bonding effect between the layers was not good but the separation between the fiber and resin is not observed, implying the impregnation effect was great.



Figure 16. Zeiss Gemini-560 field emission scanning electron microscopy.

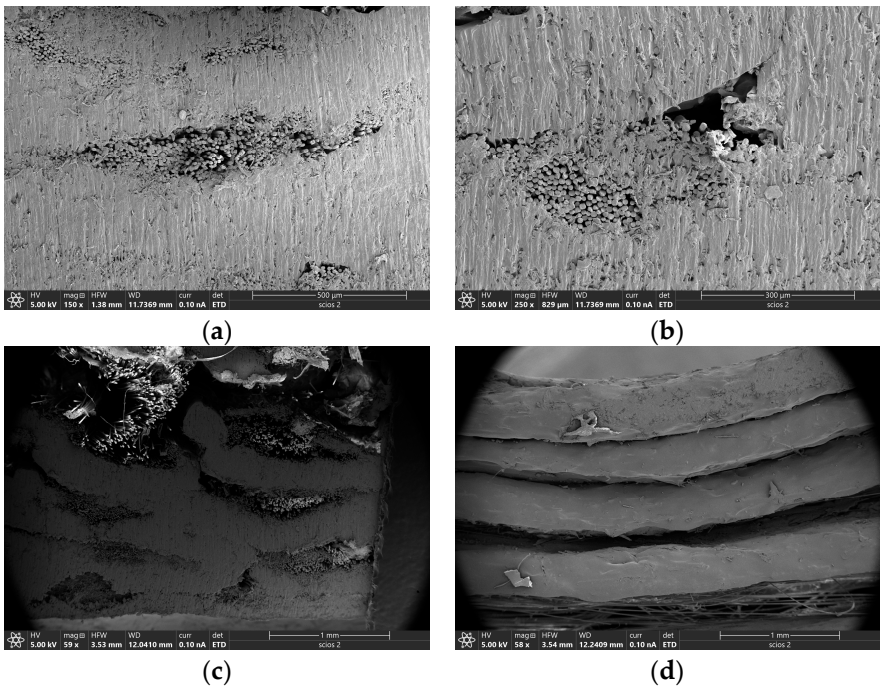


Figure 17. SEM photo: (**a**) cross section before the shear test; (**b**) void and gap; (**c**) cross-sectional view of failure specimen; (**d**) side view of failure specimen.

3.2.5. Thermal–Mechanical Test

The specimen's dynamic mechanical analysis (DMA) and thermogravimetry analysis (TGA) tests were carried out to evaluate the material's mechanical stability under high

temperature. The two test curves are shown in Figures 18 and 19, respectively. In the DMA test curve, the storage modulus begins to decrease after 50 °C until 225 °C and at 120 °C the storage modulus almost loses half, which means under dynamic loads and high temperature the strength performance cannot be maintained at a high level. From the TGA test curve, it can be seen that the specimen begins to lose mass at around 275 °C while the mass ends with 46.68% at 500 °C. This indicates the PP resin starts to evaporate and decompose after 275 °C.

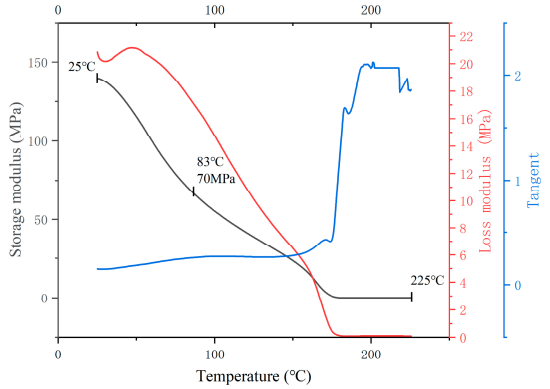


Figure 18. DMA test curve.

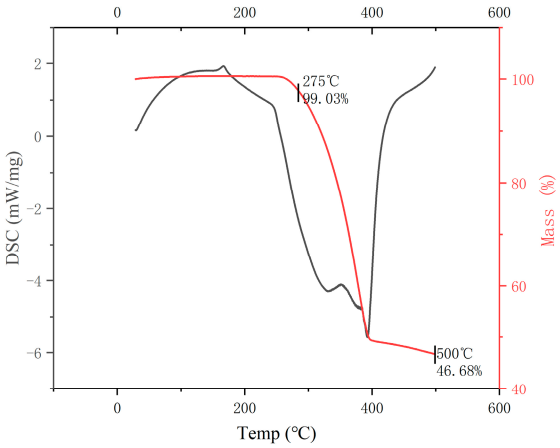


Figure 19. TGA test curve.

4. Discussion

The equipment succeeded in fabricating the groove structure and from the interlaminar shear test results, the best mechanical performance reaching the interlaminar shear strength of 6.694 MPa occurred in the group of 90° fiber orientation. This is because at 90°, the fiber was perpendicular to the load-bearing direction, which completely made full use of the fiber's strength. Following that, it was found that the smaller the thickness of the layer, the greater the ILSS was. As the thickness of one layer decreased, it meant at the same thickness, more layers were stacked, which led to more fiber at this direction. Hence, the mechanical strength was improved. For heating temperature, it mainly affected the fluidity of the PP resin and the second impregnation effect of the glass fiber and PP resin. Through the primary test, in the selected range of the heating temperature, the printing quality was good.

From the SEM photo, overall the glass fiber and PP resin's bonding quality was good while in some areas the gap and void, which results in the decrease in the mechanical performance, could be observed. After mechanical failure, the typical interlayer debonding was obvious, indicating the processing method still needs to be improved. However, no

separation between the glass fiber and PP resin occurred, proving that it is a feasible method for making prepreg wire through an online impregnation printing device.

Through the thermal–mechanical tests, DMA and TGA, the dynamic mechanical performance and stability of the samples under high temperature were obtained. The mechanical strength was almost lost at 175 °C and when it came to 120 °C, only half of the strength could be saved. In the TGA, when it lost all the mechanical strength at 225 °C in the DMA, the weight still maintained at almost 100% and began to lose at around 275 °C. Therefore, it is not recommended to be used under high temperature in the composite material combination of glass fiber and PP resin.

Although the combining method for groove structure was realized and the suitable fiber orientation was found, the number of the experiments was not sufficient. In addition, more factors like the mold heating temperature which may influence the interlayer's bonding effect shall be explored.

5. Conclusions

In this paper, a method combining filament winding and 3D printing was presented and the corresponding equipment was designed, in order to achieve the fabrication of the groove structure. Also, the processing trajectory was designed for this combining method application. The interlaminar shear strength of the load-bearing parts was tested to investigate the processing parameters, fiber orientation, layer thickness and heating temperature's influence on the strength. The results showed that the fiber orientation perpendicular to the load improved the ILSS most. SEM photos were taken to provide an insight of the micromorphology of the specimen and the failed sample, from which it was drawn that the impregnation of the prepreg wire was good while the interlayer bonding still needed to be improved. To further study the composite groove structure's application under high temperature, two thermal test were carried out. For the composite used in this paper, it was not suitable to be applied in a high temperature situation.

All in all, this paper offered a feasible method to fabricate a complex structure like the groove structure combining the two composite manufacture methods of filament winding and 3D printing. However, the presented method still has room to be improved. For enhancing the mechanical performance of the groove structure, taking advantage of winding and designing more printing trajectory based on mechanics to further improve the structure's strength on the load-bearing direction should be advanced. Moreover, other processing parameters like the mold heating temperature can be explored. And for application under high temperature, the resin matrix can be changed to polyether-ether-ketone or others.

Author Contributions: Conceptualization, C.C. and S.H.; methodology, S.H. and C.C.; software, C.C. and J.L.; validation, C.C. and J.L.; formal analysis, J.L. and S.S.; investigation, S.H. and S.T.; resources, S.T.; writing—original draft preparation, S.H. and C.C.; writing—review and editing, Z.H., S.S. and Q.C.; supervision, Z.H. and S.S.; project administration, X.R. and S.T. All authors have read and agreed to the published version of the manuscript.

Funding: This research received no external funding.

Data Availability Statement: Data are contained within the article.

Conflicts of Interest: Author Jiaqi Liu was employed by Chang Guang Satellite Technology Co., Ltd. The remaining authors declare that the research was conducted in the absence of any commercial or financial relationships that could be construed as a potential conflict of interest.

References

1. Deng, H.; Chen, W.; Bai, G.; Dong, S. Experimental Study on shear Resistance of Aluminum Alloy plate Rivet with ring Slot. *J. Build. Struct.* **2016**, *37*, 143–149. [CrossRef]
2. Fang, K.; Xiang, Z.T.; Zhang, J.; Yang, L.; Hu, G.H.; Cui, K.J.; Xu, J. Additive Manufacturing and Application of 3D printing Carbon Fiber reinforced plastics and composites. *New Mater. Ind.* **2017**, *1*, 31–37. [CrossRef]

3. Wang, J.; Geng, Z.; Du, Z.; Gu, H.; Suo, H. Research on High precision Closed loop Tension Control System of Fiber Winding Machine. *Fiber Compos. Mater.* **2021**, *38*, 52–55. [CrossRef]
4. Zhang, X.; Shu, H.; Xing, P.; Zhu, G.; Zhu, J. Structural Reliability Evaluation Method of fiber Wound composite and its application. *Propuls. Technol.* **2022**, *43*, 177–186. [CrossRef]
5. Sorrentino, L.; Anamateros, E.; Bellini, C.; Carrino, L.; Corcione, G.; Leone, A.; Paris, G. Robotic filament winding: An innovative technology to manufacture complex shape structural parts. *Compos. Struct.* **2019**, *220*, 699–707. [CrossRef]
6. Ma, Q.; Ge, J.; Rejab, M.; Sun, B.; Ding, Y.; Nie, X.; Pang, H. Fabrication of the carbon fiber reinforced plastic(CFRP) cone tube through the laboratory-scale 3-axis winding machine. *Mater. Today Proc.* **2021**, *46*, 1645–1651. [CrossRef]
7. Dawson, N.; Donna, K. Mae West: Pipe dream in munich. *High Perform. Compos.* **2011**, *19*, 46–53.
8. Błachut, A.; Wollmann, T.; Panek, M.; Vater, M.; Kaleta, J.; Detyna, J.; Hoschützky, S.; Gude, M. Influence of Fiber Tension during Filament Winding on the Mechanical Properties of Composite Pressure Vessels. *Compos. Struct.* **2023**, *304*, 116337. [CrossRef]
9. de Menezes, E.A.; Lisbôa, T.V.; Almeida, J.H.S.; Spickenheuer, A.; Amico, S.C.; Marczak, R.J. On the winding pattern influence for filament wound cylinders under axial compression, torsion, and internal pressure loads. *Thin-Walled Struct.* **2023**, *191*, 111041. [CrossRef]
10. Adi, R.K.; Das, S.; Muflikhun, M.A. Design and analysis of filament winding machine for cylinder manufacturing process using glass fiber composite. *Mater. Today Proc.* **2022**, *66*, 2904–2907. [CrossRef]
11. Früh, N.; Knippers, J. Multi-stage filament winding: Integrative design and fabrication method for fibre-reinforced composite components of complex geometries. *Compos. Struct.* **2021**, *268*, 113969. [CrossRef]
12. Ma, X.; Yang, R.; Kang, N.; Wang, R. Research on polylactic acid composites based on 3D printing technology. *J. Jilin Inst. Chem. Technol.* **2022**, *39*, 10–14. [CrossRef]
13. Zhang, F.; Ma, G.F.; Tan, Y.G. The Nozzle Structure Design and Analysis for Continuous Carbon Fiber Composite 3D Printing. In Proceedings of the International Conference on Advanced Design and Manufacturing Engineering (ICADME 2017), Shenzhen, China, 10–11 May 2017; pp. 193–199.
14. Tian, X.; Liu, T.; Yang, C.; Wang, Q.; Li, D. Interface and performance of 3D printed continuous carbon fiber reinforced PLA composites. *Compos. Part A Appl. Sci. Manuf.* **2016**, *88*, 198–205. [CrossRef]
15. Ming, Y.; Duan, Y.; Wang, B.; Xiao, H.; Zhang, X. 3D printing of high-performance fiber-reinforced resin matrix composites. *Aerosp. Manuf. Technol.* **2019**, *62*, 34–38. [CrossRef]
16. Reuter, J.; Böcking, J.; Engel, B. End-forming of Continuous Fibre-reinforced Thermoplastic Tubes. *Procedia Manuf.* **2020**, *47*, 190–196. [CrossRef]
17. Hou, Z.; Tian, X.; Zhang, J.; Zhe, L.; Zheng, Z.; Li, D.; Malakhov, A.V.; Polilov, A.N. Design and 3D printing of continuous fiber reinforced heterogeneous composites. *Compos. Struct.* **2020**, *237*, 111945. [CrossRef]
18. Li, Y.; Liu, S. Rapid prototyping of continuous carbon fiber reinforced polylactic acid composites by 3D printing. *J. Mater. Process. Technol.* **2016**, *238*, 218–225. [CrossRef]
19. Prüß, H.; Vietor, T. Design for Fiber-Reinforced Additive Manufacturing. *J. Mech. Des.* **2015**, *137*, 111409. [CrossRef]
20. Zhang, P.; Sun, S.; Duan, J.; Fu, H.; Han, Z.; Geng, H.; Feng, Y. Line width prediction and mechanical properties of 3D printed continuous fiber reinforced polypropylene composites. *Addit. Manuf.* **2023**, *61*, 103372. [CrossRef]
21. Rakhshbahar, M.; Sinapius, M. A Novel Approach: Combination of Automated Fiber Placement (AFP) and Additive Layer Manufacturing (ALM). *J. Compos. Sci.* **2018**, *2*, 42. [CrossRef]
22. Velu, R.; Vaheed, N.M.; Venkatesan, C.; Raspall, F.; Krishnan, M. Experimental investigation on fabrication of thermoset prepreg composites using automated fibre placement process and 3D printed substrate. *Procedia CIRP* **2020**, *85*, 296–301. [CrossRef]
23. Parandoush, P.; Tucker, L.; Zhou, C.; Lin, D. Laser assisted additive manufacturing of continuous fiber reinforced thermoplastic composites. *Mater. Des.* **2017**, *131*, 186–195. [CrossRef]
24. Beijing FRP Research and Design Institute. Determination of Interlayer Shear Strength of Fiber Reinforced Plastics by Short Beam Method. In *Industry Standard-Building Materials*; JC/T 773-2010.2010-11-22; Beijing FRP Research and Design Institute: Beijing, China, 2010.
25. Hao, L.; Yu, H. Analysis of the use of orthogonal experimental design table. *Editor. J.* **2005**, *5*, 334–335. [CrossRef]

Disclaimer/Publisher's Note: The statements, opinions and data contained in all publications are solely those of the individual author(s) and contributor(s) and not of MDPI and/or the editor(s). MDPI and/or the editor(s) disclaim responsibility for any injury to people or property resulting from any ideas, methods, instructions or products referred to in the content.